LANGMUIR

Article

pubs.acs.org/Langmuir

Solution-Stable Colloidal Gold Nanoparticles via Surfactant-Free, Hyperbranched Polyglycerol-*b*-polystyrene Unimolecular Templates

James Iocozzia and Zhiqun Lin*

School of Materials Science and Engineering, Georgia Institute of Technology, Atlanta, Georgia 30332, United States

Supporting Information

ABSTRACT: Hyperbranched polyglycerol-*block*-polystyrene copolymers, denoted HPG-*b*-PS, are synthesized and employed as a new and effective unimolecular template for synthesizing colloidal gold (Au) nanoparticles. The coordination of noble metal precursors with polyether within the inner HPG core and subsequent in situ reduction enables the formation of well-dispersed and stable PS-capped Au nanoparticles. The inner HPG core is produced via ring opening multibranching polymerization (ROMBP) and subsequently converted into atom transfer radical polymerization (ATRP) macroinitiators for the controlled growth of polystyrene (PS) arms possessing low polydispersity (PDI < 1.31). An initial investigation into the templating parameters of HPG-*b*-PS was undertaken by producing templates with different arm numbers (98 and 117) and different PS chain lengths (i.e., molecular weight = 3500−13400 g/mol). It was found that the PS chain length and solvent conditions affect the quality of the resulting PS-capped colloidal Au nanoparticles. This work demonstrates, *for the first time*, a simple, lower-cost approach for templating nonpolar solvent-soluble PS-capped Au nanoparticles on the order of 10−30 nm in diameter.

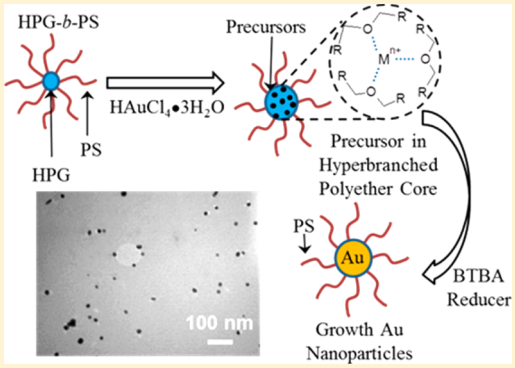

INTRODUCTION

The production of nanocomposites for various end uses has matured past mere lab scale curiosities to relevant application-driven research. Thus, the question of scalability and cost are two essential factors governing practical research development. Established methods for the production of nanoscale materials include chemical vapor deposition (CVD), atomic layer deposition (ALD), and other sputtering-type approaches. Requiring ultrapure starting materials and cleanroom conditions, these techniques are expensive to employ. Among many alternatives, non-micelle templating of nanostructures via solution chemistry (in the same class as hydrothermal and solvothermal reactions) has emerged as a low-cost, readily scalable approach. Previous work in this area has utilized various biological and synthetic templates (unimolecular and self-assembling) to produce inorganic nanostructures, including viruses,[1−3] cylindrical polymer bottle brushes,[4,5] polyelectrolyte-containing microspheres[6] and polyelectrolyte-containing starlike copolymers,[7] self-assembling bioorganic and inorganic structures,[8−11] and DNA-templating.[12−15] It should be emphasized that many more templating strategies exist, but they are dissimilar to those related to this work which focuses on unimolecular, synthetic, and non-self-assembly processes.

In the case of starlike polymeric templates, efforts to improve the regularity, arm number, and arm type are important for conferring the necessary templating functions as well as stability of the resulting nanocomposite to prevent aggregation, subsequent reaction, and degradation. One approach to addressing these requirements is the development of perfect dendrimer templates. Early dendrimeric templating has focused on amino- and imine-containing dendrimers to nucleate catalytically active metal nanoparticles.[16,17] While dendrimers afford a more precise template structure, higher molecular weights are challenging to reach due to the generation-based growth which is tedious and time-consuming. An alternative to dendrimers employs multisite initiators, including β-cyclodextrin (containing 21 hydroxyl groups),[7] small polyols (possessing three to six hydroxyl groups),[18,19] and inorganic polyhedral oligomeric silsesquioxane (POSS) (possessing eight or more hydroxyl groups if bridged aggregates),[20] that have been modified to serve as "grafting-from" initiators for polymerizations. The formation of regular starlike initiators has been greatly improved by the parallel development of controlled polymerization techniques, including atom transfer radical polymerization (ATRP).[21,22] ATRP is a popular choice for producing well-defined polymer chains with low polydispersity. Owing to the low cost of the copper-based catalysts used and the ease of separation from the products via filtration and the mild conditions required (below 90 °C, neutral pH), it is an attractive approach for polymerizations. Since several established, one-step strategies exist for converting polyols to multisite ATRP initiators (i.e., ATRP macroinitiators), it is a natural approach to use in the production of starlike copolymer templates of diverse compositions. These strategies offer simple

Received: May 13, 2016
Revised: June 24, 2016
Published: June 30, 2016

DOI: 10.1021/acs.langmuir.6b01830
Langmuir 2016, 32, 7180−7188

approaches to multisite initiators, but the number of initiation sites is typically low (less than 10) and fixed for any given material class. Thus, it is desirable to have multisite polyol initiators that can be functionalized for ATRP where the number of initiation sites can also be tuned to any desired value while maintaining low cost, scalability, and low toxicity. Hyperbranched polyglycerols (HPG) offer such a solution.

Hyperbranched polyglycerols are an attractive class of biocompatible, water-soluble polymers possessing a large number of hydroxyl groups and ether linkages. Unlike dendrimer templating approaches, HPG can be produced in large quantities via single-pot reactions from inexpensive commercially available materials (glycidol monomer, sodium methoxide base, and 1,1,1-tris(hydroxymethyl)propane (TMP) initiator) in a relatively simpler fashion. Since their initial discovery, HPG have been promising for many applications. Much has been done to address the challenges associated with their synthesis via uncatalyzed ring opening multibranching polymerization (ROMBP) of glycidol as detailed in Scheme 1.[23−27] The scheme illustrates the complicated structure of a general HPG molecule containing the characteristic core structure and four different repeat units within the polyether−polyol structure denoted terminal (T), dendritic (D), linear-13 (L_{13}), and linear-14 (L_{14}). Frey, Sunder, Brooks et al. have introduced strategies, including slow monomer addition (SMA), improved reactor design, and sequential ROMBP,[28] to produce higher molecular weight HPG with improved degrees of branching (i.e., more terminal and dendritic units and less linear units) while maintaining a low polydispersity index (PDI < 1.5).

Scheme 1. General Scheme for the Ring Opening Multibranching Polymerization of HPG[a]

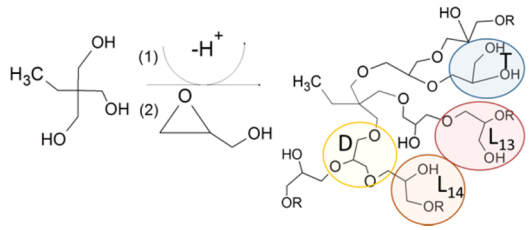

[a]The 1,1,1-tris(hydroxymethyl)propane (TMP) initiator (left) is deprotonated and the epoxide-containing glycidol monomer is slowly added. How the monomer adds dictates the type of repeat unit formed in the growing HPG structure defined as dendritic (D), terminal (T), linear-13 (L_{13}), and linear-14 (L_{14}).

In contrast to perfect dendrimers which require tedious, time-consuming, and expensive protection/deprotection chemistry, HPG can be produced in large single-pot reactions and are equally amenable to subsequent chemical modification as dendrimers. Moreover, the wealth of chemical modification techniques applied to HPG macroinitiators is impressive. The surface hydroxyl groups can be deprotonated and subjected to additional ring opening reactions to produce hydrophilic HPG-*b*-poly(ethylene oxide) type star copolymers,[29,30] functionalized with click moieties[31] or converted to ATRP macroinitiators for the polymerization of many acrylate monomers, leading to amphiphilic star copolymers[32−35] with added functionality such as cross-linking, hydrogel formation, and improved solubility in different solvents (polar, nonpolar, aqueous, etc.). Given the large potential for useful chemical functionality and relatively facile methods, HPG-based templates have emerged as a natural choice for unimolecular templating of inorganic nanoparticles.

To date, there have been only a handful of reports employing HPG-based templates in the synthesis of inorganic structures. One study focused on the partial olefinic functionalization of HPG for use in nucleating palladium nanoparticles.[36] The work relies on the coordination of metal precursors to the remaining hydroxyl groups for subsequent reduction. Partial capping with the relatively small olefinic capping agent is a good approach.[36] However, partial capping is nonspecific. It does not readily enable control over the size of the capping layer, and it often relies on the random distribution of residual hydroxyl groups to coordinate with metal precursors. Another study grows a layer of HPG on the surface of premade nanoparticles (surface-initiated ROMBP).[37] Subsequently, the hydroxyl groups are modified with an anhydride to produce carboxylic acid terminated HPG which coordinates with metal ions in a similar fashion to poly(acrylic acid) in other template materials.[7,38−43] In two related studies, a linear multimolecular templating approach is employed that relies on ether chemistry for coordinating with metal precursor ions.[44,45] Both studies utilize a linear poly(3-hexylthiophene) (P3HT) derivative, 2,2-(ethoxyethoxy)ethoxy-modified polythiophene (P3EEET), whose side chains have been converted from hexyl chains to oligomeric ether groups. These ether groups are then used to coordinate with Au or Zn ions for in situ reduction/condensation to the respective metallic and inorganic components. The modified linear P3EEET successfully templates particles; however, the monomer synthesis procedure is quite tedious and the use of multimolecular linear P3EEET templates reduces the control of size and likely affects the solution stability of the resulting nanocomposites.[38,39] In another related work, HPG was used to stabilize multiple nanoparticles in aqueous environments during synthesis.[46] This study supports the versatility of HPG-based templating; however, this approach may have long-term stability issues as well as difficulties with film formation due to multiple particles being stabilized by multiple HPG molecules in an essentially random fashion. Lastly, a few previous works investigated HPG-*b*-PS and HPG-*b*-mixed arm polymers possessing lower degrees of ATRP functionalization.[47−49] The lower degrees of functionalization likely made such polymers less equipped to serve as templates, but nonetheless heavily informed the present work.

Herein, we report the implementation of ROMBP and ATRP to produce low-cost multiarm hyperbranched polyglycerol-*block*-polystyrene (HPG-*b*-PS) block copolymers which are subsequently investigated for their ability to template the formation of Au nanoparticles. Unlike previous linear polymer templating approaches, this work demonstrates, *for the first time*, the use of the unimolecular hyperbranched core in HPG-*b*-PS copolymers to sequester Au ions primarily via polyether coordination and facilitate their in situ reduction into Au nanoparticles capped with PS chains. The resulting system shows excellent long-term solution stability in organic solvents. The effects of the molecular weight of the PS arms and the solvent type were also studied to optimize the reaction conditions and verify the templating functionality of hyperbranched HPG-*b*-PS. The synthesis procedure for the template and the resulting colloidal nanoparticles is simple, reproducible, and likely generalizable to guide the nucleation and growth of other metal and metal oxide systems quickly and at low cost. The PS capping layers make such colloidal systems applicable

DOI: 10.1021/acs.langmuir.6b01830
Langmuir 2016, 32, 7180−7188

to thin film and interfacial deposition via simple wet deposition techniques such as spin coating and dip coating.

EXPERIMENTAL SECTION

Materials. 2-Bromoisobutyryl bromide (BIBB, 98%), 2,2-bipyridyl (BDY, 99%), 1-methyl-2-pyrrolidinone (*N*-methylpyrrolidinone (NMP), 98%), glycidol (96%), and gold(III) chloride hydrate ($HAuCl_4{\cdot}3H_2O$, 99%) were purchased from Sigma-Aldrich and used as received unless otherwise noted. NMP was mixed with CaH_2 overnight and distilled under vacuum prior to use. Glycidol was distilled under vacuum immediately prior to use. Styrene (St, 99% stabilized with 15 ppm 4-*tert*-butyl catechol), sodium methoxide (NaOMe, 98%), borane *tert*-butylamine complex Au ion reducer (BTBA, 97%), benzyl alcohol (BA, 99%), and 1,1,1-tris-(hydroxymethyl)propane (TMP, 98%) were purchased from Alfa Aesar and used as received unless otherwise noted. Styrene was distilled to remove polymerization inhibitor prior to use. Dimethylformamide (DMF, solvent grade) and methanol (MeOH, solvent grade) were purchased from BDH and distilled prior to use and stored over activated molecular sieves. Bis(methoxyethyl) ether (diglyme, 99%) was purchased from Acros Organic and used as received.

Synthesis of Hyperbranched Polyglycerols (HPG). The ROMBP reactor was prepared by attaching an eternally powered Teflon stirrer into a Teflon bearing attachment in the top of a three-neck flask and placed in a temperature-controlled oil bath. To the left port of the flask, a syringe pump needle was attached. To the right port, the argon inlet and vent was attached. An amount of the TMP initiator and KOMe was added to the reactor and heated to 80 °C to form a melt. This was reacted for 60 min to remove residual water and methanol. Benzene was then added and the reactor was dried under vacuum. In some experiments, a small amount of diglyme was added to redissolve the activated initiator. In most experiments a measured amount of dry NMP was added to redissolve the initiator. Freshly distilled glycidol (50/50 weight ratio in dry NMP) was then loaded into the syringe pump and injected into the reactor at a specified rate, temperature, and stirrer speed. The reaction then proceeded for a specified period of time under inert argon atmosphere. After the reaction, NMP was distilled off and the product was redissolved in methanol. This product was then precipitated in acetone, collected, and purified twice more to yield the final HPG product (yield: 30% for HPG10 and 37% for HPG7). ^{1}H NMR (DMSO-d_6) δ (ppm): 0.91 (s, 3H, methyl group of TMP); 1.45 (s, 2H, $-CH_2-$ bridge group of TMP); 3.4−4.0 (m, 5H, HPG backbone). Inverse-gated carbon NMR, IG ^{13}C NMR, (DMSO-d_6) δ (ppm): 79.5−80.5 (L_{13}); 78−79 (D), 72−73 ($2L_{14}$); 70.5−71.5 (2D, 2T); 68−70 (L_{13}, L_{14}); 62.5−63.5 (T); 61−62.5 (L_{13}). Reaction details for HPG synthesis can be found in Table S1 of the Supporting Information (numbers denote different reactor conditions). A sample calculation of the degree of branching (DB) and structural breakdown from IG ^{13}C NMR are detailed in Figure S1 and Table S2 of the Supporting Information. Yields for primary HPG synthesis are deliberately low to prevent cross-coupling and increased PDI.

Formation of HPG-Br Macroinitiators (MI). The HPG macroinitiators (i.e., brominated HPG (HPG-Br)) were formed by reacting BIBB with the hydroxyl groups of HPG in an esterification reaction. Different HPG samples were prepared (i.e., HPG1, HPG2, and so on) as summarized in Table S1 of the Supporting Information. In a representative procedure, 4.06 g of HPG7 (0.055 mol of −OH) was dried in a vacuum oven overnight followed by azeotropic distillation with 40 mL of toluene. HPG7 was dissolved in dry NMP (20−30 mL) and chilled to 0 °C. A 8.12 mL volume of BIBB (0.066 mol) was added dropwise to HPG7 solution under magnetic stirring over 30 min and allowed to react for 24 h. The crude product was washed with $NaHCO_3$ (5 wt % in deionized (DI) water) three to four times until bubbling stopped, washed with DI water 2−3 times, dried overnight with $MgSO_4$, filtered, and dried overnight under vacuum (55 °C) to yield a brown highly viscous product (yield: 75% for HPG10-Br and 81% for HPG7-Br). ^{1}H NMR ($CDCl_3$) δ (ppm): 1.92 (s, 6H, $-C(CH_3)_2-$Br (primary bromination signal); 4.1−4.2, 4.25−4.4, 4.5−4.6, 5−5.2, 5.25−5.4 (m, 6H, $-CH_2-$ and $-CH_2-CH(-O-)-CH_2-$ near bromine in HPG backbone). In all HPG brominations, BIBB was added in a 1:1.2 molar ratio −OH:BIBB.

Preparation of Unimolecular HPG-*b*-PS Copolymer Templates. ATRP of styrene was performed in bulk at 90 °C. A 150 mL Schlenk flask was charged with an amount of HPG-*b*-PS macroinitiator, 80% of the required amount of freshly distilled and dried styrene monomer, and a magnetic stirrer. In a separate vial, an amount of CuBr cocatalyst was dispersed in the remaining styrene. To this, an amount of PMDETA cocatalyst was added dropwise to the CuBr solution and sonicated to produce the catalyst solution. The catalyst was added to the Schlenk flask and sealed. The flask then underwent three freeze−pump−thaw cycles under N_2 atmosphere. The flask reacted at temperature for a given amount of time. The flask was quenched with liquid nitrogen, diluted with THF, and passed through a neutral alumina column to remove catalyst. The crude product was precipitated in a cold solution of 50/50 methanol and water. The product was redissolved and precipitated twice more. The purified product was then stirred with $MgSO_4$ overnight, filtered, and dried in a vacuum oven for 48 h. Details for the different ATRP experiments are in Table S3 of Supporting Information. ^{1}H NMR ($CDCl_3$) δ (ppm): 0.70−0.95 (s, 6H, $-C(CH_3)_2-$PS); 1.25−2.15 (m, 3H, $-CH_2CH-$ of PS); 2.80−4.0 (m, 5H, $-CH-$ and $-CH_2-$ of HPG core); 4.45−4.65 (d, 1H, CH_2-CH(Ph)−Br); 6.35−7.35 (m, 5H, $-C_6H_5$ of PS). The different HPG-*b*-PS samples are usefully labeled based on the molecular weight of the HPG core, the number of PS arms, and the length of the PS arms. The molecular weight of the grown chains was determined by cleaving the ester linkages attaching the chains to the HPG core by refluxing the HPG-*b*-PS copolymers in THF under basic conditions. The resulting solutions were precipitated in water, filtered, and dried prior to analysis.

In Situ Synthesis of PS-Capped Colloidal Au Nanoparticles. Several conditions for templating Au nanoparticles with HPG-*b*-PS copolymers were investigated. In all cases, a molar ratio of 1:7 was maintained between the Au precursor and the borane *tert*-butylamine complex (BTBA) reducer used to reduce Au ions to metallic Au. The BTBA precursor solution was prepared in small batches by dissolving 0.0393 g of $HAuCl_4{\cdot}3H_2O$ in 1 mL of dry DMF. The reducer solution was prepared in small batches immediately prior to each experiment by dissolving 0.061 g of BTBA in 1 mL of dry DMF. For samples Au1@HPG9.3k-*b*-98PS4.5k, Au2@HPG9.3k-*b*-98PS4.5k, Au3@HPG9.3k, and Au4@HPG9.3k, 20 h of stirring was allowed for precursor incorporation prior to in situ reduction and allowed to react for 30 min prior to termination. For samples Au5@HPG9.3k-*b*-98PS4.5k, Au6@HPG9.3k-*b*-98PS4.5k, Au7@HPG9.3k, and Au8@HPG9.3k, 120 h of stirring was allowed for precursor incorporation into the inner HPG block prior to in situ reduction and allowed to react for 10 min prior to termination. For samples Au9@HPG9.3k-*b*-98PS4.5k, Au10@HPG9.3k-*b*-98PS4.5k, and Au11@HPG9.3k-*b*-98PS4.5k, the reaction solvent type was varied from 9:1, to 8:2, to 6:4 DMF:BA (v/v), respectively. Gradually increasing the content of BA gradually reduces the overall solubility of the PS chains of the HPG-*b*-PS templates. Previous work with templating via a different nanoreactor approach also showed the importance of the solvent type in yielding nanoparticles.[7] For samples Au12@HPG9.3k-*b*-98PS7k, Au13@HPG9.3k-*b*-98PS13.4k, Au14@HPG12.6k-*b*-117PS3.6k, and Au15@HPG12.6k-*b*-117PS5k, the length of the arms was varied to investigate its effect. Details of the reaction conditions can be found in Tables S3 and S4 of the Supporting Information.

Characterization. Absolute molecular weights of polymers and structural verification were determined by ^{1}H NMR operating on a Varian VXR-400 (400 MHz) Unity Innova spectrometer with a Nalorac quad-probe. T^1-inversion recovery and inverse-gated carbon NMR (IG ^{13}C NMR) were performed on the same instrument to determine necessary scan times, determine the structural composition of HPG samples, and calculate the degree of branching (DB). Gel permeation chromatography was performed on a Shimadzu GPC setup (RID-10A refractive index detector, CTO-20A column oven, and LC-20A chromatograph pump). For HPG polymers only, DMF with LiCl additive was used as the mobile phase (calibrated with linear PEO

DOI: 10.1021/acs.langmuir.6b01830
Langmuir 2016, 32, 7180−7188

Table 1. Molecular Weight and Structural Characterization Parameters of HPG

sample	$M_{n,HNMR}$[a] (g mol^{-1})	$M_{n,GPC}$[b] (g mol^{-1})	$M_{w,GPC}$[b] (g mol^{-1})	PDI	no. −OH[a]	T[c] (%)	D[c] (%)	L_{13}[c] (%)	L_{14}[c] (%)	DB[d]	−Br[e] (%)
HPG2	7200	4200	6200	1.4	91	47	22	15	16	59	88
HPG7	12600	5900	18000	3.2	170	38	18	12	32	45	69
HPG10	9300	7200[f]	10000[f]	1.38[f]	126	34	23	18	25	52	78

[a]Average value determined by dividing the integrated HPG backbone proton signal by the integrated proton signal of the initiator core using eq 1. [b]DMF GPC mobile phase contains 0.1% LiCl additive and uses linear PEG calibration standards. [c]HPG terminal (T), dendritic (D), linear type 1 (L_{13}), and linear type 2 (L_{14}) determined by integrating respective signals obtained in IG ^{13}C NMR spectra (see Figure S1 and Table S2 for representative spectra and calculation). [d]Degree of branching (DB) calculated by eq 2 introduced by Frey.[28] [e]Percent esterification via BIBB calculated by eq 3 introduced by Huang.[49] [f]Values based on brominated analogue.

standards). For HPG-*b*-PS copolymer templates, THF was used as the mobile phase (calibrated with linear PS standards). A Phenomenex phenogel linear column with mixed pore size beads was used in GPC measurements (MW range 200−2 × 10^6 g mol^{-1}). UV−vis was performed on a Shimadzu UV-2600 spectrometer with quartz cuvettes (10 mm path length). HPG-*b*-PS template and PS-capped Au nanoparticle characterization were performed on a Renishaw inVia Raman microscope with 785 nm excitation wavelength. The elemental composition of Au nanoparticles was verified by X-ray diffraction on a PANalytical XRD with Cu Kα radiation (λ = 0.154 nm).

RESULTS AND DISCUSSION

Effect of Stoichiometry, Solvent, Cosolvent, and Degree of Deprotonation on HPG. Three different molecular weights of HPG were synthesized for use as ATRP macroinitiators after bromination of HPG (see the Experimental Section). Ultimately HPG2-Br was not employed as a macroinitiator for this study due to its relatively low number of ATRP initiation sites compared to the other two as well as its relatively low yield during ROMBP. Despite having the longest polymerization time and slowest monomer injection rate, it still had the lowest molecular weight due largely to the low degree of deprotonation of the initiator. It is nonetheless illustrative for the purposes of characterization as it provides clear peaks in IG ^{13}C NMR. With an adjustment of the reaction conditions to include a higher initial degree of deprotonation, faster monomer injection rate, and higher proportion of NMP solvent (improved solubility), higher molecular weight HPG7 and HPG10 were obtained (see Table S1 in Supporting Information for the details of the different synthesis techniques of HPG7 and HPG10, where numbers denote different procedures). The trade-off, however, is that when higher molecular weights are attained, there is a pronounced increase in the molecular weight distribution, a reduction in the number of dendritic and terminal units, and an increase in the number of linear units as demonstrated for HPG7. A comfortable balance was obtained for HPG10 in which a substantial number of initiation sites were produced without a compromise in the molecular weight. Degree of polymerization (DP) and degree of branching (DB) were calculated by eqs 1 and 2 as follows and summarized in Table 1:

$$\mathrm{DP} = \frac{\frac{A_{\text{polyether core}}}{5} - 2A_{\text{methyl}}}{\frac{A_{\text{methyl}}}{3}} \quad (1)$$

$$\mathrm{DB} = \frac{2D}{2D + L_{13} + L_{14}} \quad (2)$$

where $A_{\text{polyether core}}$ is the integrated area of the HPG backbone proton signals, A_{methyl} is the integrated area of the methyl group of the TMP initiator core, and D, L_{13}, and L_{14} are the integrated areas of the IG ^{13}C NMR spectrum of HPG.

Thus, HPG10-Br (i.e., HPG10 after bromination, see the Experimental Section) served as the principal macroinitiator for this work. HPG7-Br was also employed to investigate the effects of arm number on the templating of Au nanoparticles. It should be noted that the investigation of the effects of arm number and length are introductory and not the main focus of this work. The long reaction time during bromination enabled a higher percentage of initiation sites to be realized than reported in previous works which typically focused on lower degrees of esterification.[47,48] In this work, the degree of esterification (i.e., to yield HPG-Br) was much larger such that most of the hydroxyl groups are converted to ATRP initiation sites. The high degree of bromination was calculated from eq 3 using the ^{1}H NMR signals for the HPG-Br macroinitiators.

$$-\mathrm{Br}\ (\%) = \frac{\frac{A_{\mathrm{Br}}}{6}}{\frac{A_{\text{polyether core}}}{5}} \quad (3)$$

where A_{Br} is the integral of the methyl group NMR signal on the BIBB-functionalized HPG-Br macroinitiator and $A_{\text{polyether core}}$ is the integral of the polyether backbone NMR intensity. By multiplying the degree of bromination with the average number of −OH present in each HPG molecule, the number of initiation sites (i.e., PS arms to be grown) can be calculated. For HPG7 and HPG 10 these values were 117 and 98, respectively.

Molecular Weight Control of HPG-*b*-PS Copolymers. Two points needed to be addressed before using the HPG-*b*-PS copolymers as templates. The first was whether or not ATRP of styrene was initiated by the HPG-Br macroinitiators. The second was whether or not the polymerizations proceeded in a living fashion that can be controlled over various molecular weights. Both points were verified by assuming the macroinitiators worked and growing various PS chain lengths from them (Figure 1a). We note that HPG7-based macroinitiators had 117 arms and HPG10-based macroinitiators had 98 arms. It was found that a massive increase in the molecular weight of HPG-*b*-PS copolymer occurred, indicating a growth from the macroinitiator as desired. Subsequently, the PS chains were cleaved from the HPG-*b*-PS template and measured via GPC to determine the polydispersity and average size (Figure 1b). In all cases, a PDI less than 1.31 and a molecular weight ranging from 3.6 to 13.4 kg/mol per arm were obtained.

Larger molecular weights of HPG-*b*-PS were avoided due to the greater chance of chain−chain coupling leading to larger polydispersity for the HPG-*b*-PS templates. This effect can already be seen for HPG9.3k-*b*-98PS13.4k (PS polymerization for 720 min) whose PDI is greater than 2. Since the number of arms is much larger than most polymers previously investigated, there is a much larger possibility for intra- and interchain coupling in this system.[41,42] Despite this, the cleaved

DOI: 10.1021/acs.langmuir.6b01830
Langmuir 2016, 32, 7180−7188

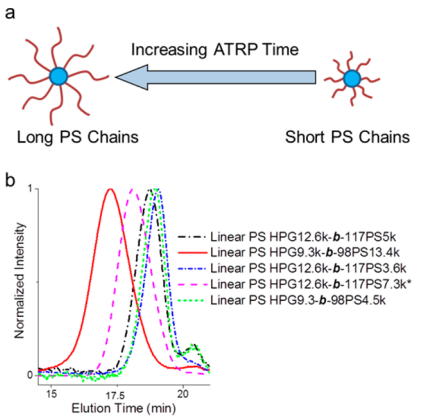

Figure 1. (a) Schematic describing the effect of reaction time on the length of the PS arms grown from the HPG-Br macroinitiators. (b) GPC traces of the cleaved linear PS chains grown via ATRP from the various HPG-Br macroinitiators. Samples showed low PDIs and unimodal distributions supporting the expected initiation mechanism and living nature of the polymerizations. The number or arms was either 117 or 98 for HPG7 or HPG10-based macroinitiators, respectively. The reaction marked with an asterisk (∗) used twice the catalyst compared to the other HPG12.6k-*b*-117PS5k template.

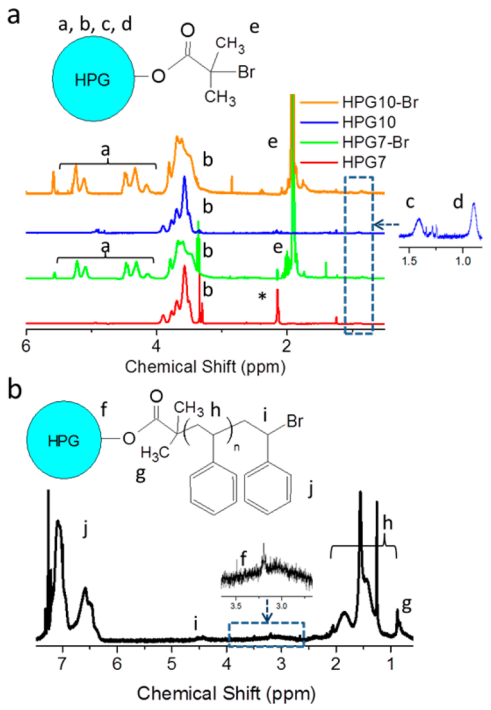

Figure 2. (a) ^{1}H NMR spectra for HPG7, HPG10, their respective brominated macroinitiators, and (b) HPG9.3k-*b*-98PS4.5k, showing both the HPG core signals and the PS chains. Residual solvent peaks denoted with an asterisk (∗).

chains are still quite monodisperse, which supports that the chains are initiated from the HPG-Br macroinitiators as desired and that the chains grow in a living fashion. The detailed molecular weight characterizations of the HPG-*b*-PS samples are summarized in Table 2. Note the sample names in Table 2 include the molecular weight of the HPG core, the number of initiation sites and the length of the PS arms.

To further establish that HPG-Br serves as an ATRP initiator in these experiments, ^{1}H NMR was used to ensure high bromination efficiency as well as verify that the core (i.e., HPG) is retained in the purported template (i.e., HPG-*b*-PS). Figure 2 summarizes the ^{1}H NMR spectra of the HPG samples as well as their macroinitiators (Figure 2a) and a representative HPG-*b*-PS copolymer sample (Figure 2b). Consistent results are observed for HPG synthesis as well as their respective brominated macroinitiators (HPG7-Br and HPG10-Br) as shown by the strong peaks found around 1.92 ppm in the NMR spectrum (peak e in Figure 2a). The low intensity peaks of the TMP initiator are also observed, thus supporting the proper initiation and ROMBP (peaks c and d in Figure 2a). In addition, the weak signals of the HPG backbone and macroinitiator core are also preserved in the spectrum for HPG9.3k-*b*-98PS4.5 (peaks f and g Figure 2b) as well as the PS chain signals (peaks j, i, and h in Figure 2b). Verification of the retention of the inner HPG core was essential prior to using HPG-*b*-PS as a template for synthesizing Au nanoparticles.

Effect of Solvent Conditions and Arm Length of HPG-*b*-PS on Templating Au Nanoparticles. Investigation into the templating ability of various HPG-*b*-PS copolymers was divided into three sections. In the first section, optimum solvent conditions were employed (pure DMF) and the importance (if any) of the chelation time was investigated. In the second section, the solvent type was varied to determine if the nanoparticles are in fact being preferentially coordinated with the polyether core and reduced in situ. In the third section, variation in the length and number of PS arms was scrutinized to examine the effective arm length for separating the different cores during coordination/reduction as well as maintaining long-term, stable nanoparticle dispersions. It is important to note that the effects of arm length and arm number are of lesser importance than the overall ability to template particles. Samples Au1@HPG9.3k-*b*-98PS4.5k and Au2@HPG9.3k-*b*-98PS4.5k allowed precursor chelation over 20 h, whereas Au5@HPG9.3k-*b*-98PS4.5k and Au6@HPG9.3k-*b*-98PS4.5k allowed precursor chelation for 120 h (see the Experimental Section). After in situ reduction, it was found that the degree of cluster formation and adjoined particles was greatly reduced for the latter two samples (Figure 3). The overall size and shape of the PS-capped Au nanoparticles did not vary significantly between the four samples which were on the order of 13 nm in diameter. Successful precursor coordination and in situ

Table 2. Summary of Parameters for HPG-Br, HPG-*b*-PS, and Cleaved PS Chains

sample	ATRP MI[a]	$M_{n,star,GPC}$[b] (g mol^{-1})	$M_{w,star,GPC}$[b] (g mol^{-1})	PDI_{star}	$M_{n,PS,GPC}$[c] (g mol^{-1})	$M_{w,PS,GPC}$[c] (g mol^{-1})	PDI_{PS}
HPG12.6k-*b*-117PS3.6k	HPG7-Br	31000	44000	1.45	3600	4400	1.23
HPG12.6k-*b*-117PS5k	HPG7-Br	134000	156000	1.16	5000	5900	1.16
HPG9.3k-*b*-98PS4.5k	HPG10-Br	32000	42000	1.31	4500	5100	1.14
HPG9.3k-*b*-98PS13.4k	HPG10-Br	127000	274000	2.16	13400	17500	1.31

[a]HPG7-Br has 117 initiation sites and HPG10-Br has 98 initiation sites which are reflected in the names of the different samples. [b]THF GPC of HPG-*b*-PS star copolymer. [c]THF GPC characterization of linear PS chains cleaved from the HPG macroinitiator.

DOI: 10.1021/acs.langmuir.6b01830
Langmuir 2016, 32, 7180−7188

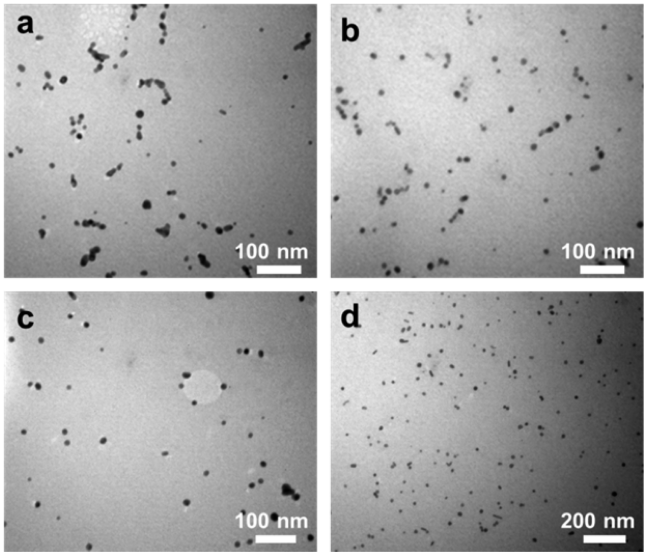

Figure 3. Transmission electron microscopy (TEM) images of Au nanoparticles templated by HPG9.3k-*b*-98PS4.5k under different conditions in optimal solvent (DMF only). (a) Au1@HPG9.3k-*b*-984.5k and (b) Au2@HPG9.3k-*b*-98PS4.5k were allowed 20 h for precursor incorporation prior to in situ reduction to produce particles with satisfactory shape and size variation (D_{Au} = 13.3 ± 3.1 nm). (c) Au5@HPG9.3k-*b*-98PS4.5k and (d) Au6@HPG9.3k-*b*-98PS4.5k were allowed 120 h for precursor incorporation prior to in situ reduction with a reduced size variation compared to first trials (D_{Au} = 13.1 ± 1.4 nm). Both Au5@HPG9.3k-*b*-98PS4.5k and Au6@HPG9.3k-*b*-98PS4.5k successfully templated the formation of Au nanoparticles; however, the longer incorporation time improved the shape quality and reduced the formation of clusters. See Tables S1 and S4 in the Supporting Information for the sample labeling clarification.

reduction is indirectly observed during the purification process of the resulting PS-capped Au nanoparticles via repeated precipitation, centrifugation, and dissolution. During precipitation, only Au ions coordinated by the HPG core and subsequently reduced in situ are integrated into the various HPG-*b*-PS templates. Thus, during centrifugation, the particles that form outside the template settle to the bottom and are removed (Figure S2). This supports the presence of the Au ion−HPG core interaction.

In addition to successful templating of individual Au nanoparticles, the resulting PS-capped Au nanoparticles showed excellent long-term stability in organic solvents with no observable sedimentation. These experiments were all performed in DMF. Prior to the addition of the reducer, the precursor ions were allowed to diffuse into the inner HPG template. The outer PS chains encapsulated the ions during the in situ reduction and prevented aggregation and sedimentation of the Au nanoparticle formed within the HPG-*b*-PS template. Additional verification of the formation of Au nanoparticles within the inner HPG core is supported by Raman and X-ray diffraction (XRD) experiments (Figures S3 and S4). Raman spectroscopy supported the formation of Au nanoparticles due to the presence of the characteristic PS signature in the PS-capped Au nanoparticles. XRD measurement showed the characteristic peaks of Au. The success rate for producing Au nanoparticles using the HPG9.3k-*b*-98PS4.5k template is high, and the method for purification of the nanocomposites (i.e., PS-capped Au nanoparticles) relies on simple precipitation of the PS capping layer.

Solvent Effects. In order to further support the nature of HPG-*b*-PS copolymers as Au templates, an investigation into the effects of solvent type on templating was also undertaken. These experiments varied the solvent composition from 9:1 DMF:BA, a relatively good solvent mixture for PS, to 6:4 DMF:BA, a relatively poor solvent mixture for PS. BA is a bad solvent for PS; the rationale is that the PS chains will collapse inward as the solvent composition worsens, thereby reducing the ability of the metal precursor ions and reducer to diffuse into the inner HPG core. The expected result then is a reduction in the degree of successful templating and/or quality of the resulting nanocomposites. Figure 4 shows TEM images of the templated PS-capped Au nanoparticles under some of the solvent compositions investigated.

The particles templated in the best solvent mixture for PS (Figure 4a) resulted in aggregate-free and well-dispersed PS-capped Au nanoparticles on the order of 15 nm which retained the characteristic plasmonic Au peak around 520 nm (Figure 5a, top). Nanoparticle templating in the intermediate solvent mixture (intermediate PS solubility) (Figure 4b) showed a

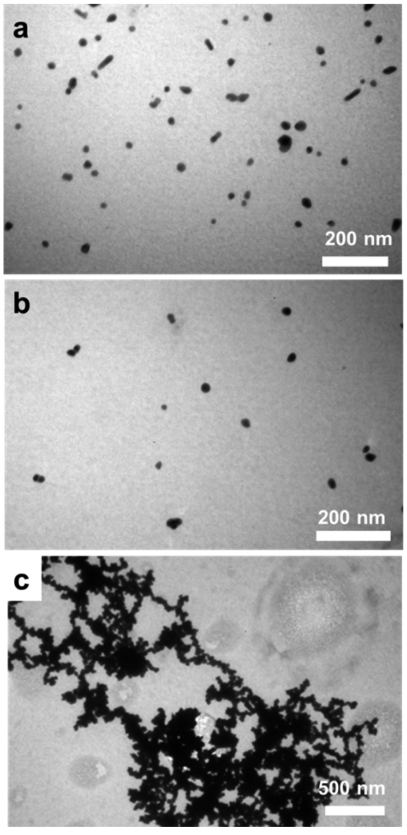

Figure 4. TEM images of PS-capped Au nanoparticles templated with HPG9.3k-*b*-98PS4.5k (i.e., HPG10 batch with PS polymerized for 150 min from the chain end of HPG) under different solvent conditions. (a) The solvent for Au9@HPG9.3k-*b*-98PS4.5k is 9:1 DMF:BA (v/v) and showed a large number of nanoparticles templated and a larger average particle diameter (D_{Au} = 18.0 ± 5.0 nm). (b) The solvent for Au10@HPG9.3k-*b*-98PS4.5k is 8:2 DMF:BA (v/v) and showed some particle templating but a reduced number due to the slightly collapsed PS chains outside of the HPG core and a larger average particle diameter (D_{Au} = 20.6 ± 6.4 nm). (c) For comparison, a control experiment was also performed with no template and demonstrated a large-scale aggregation and sedimentation. AuBTBA11 (6:4 DMF:BA) also aggregated and settled too quickly to create a TEM grid.

DOI: 10.1021/acs.langmuir.6b01830
Langmuir 2016, 32, 7180−7188

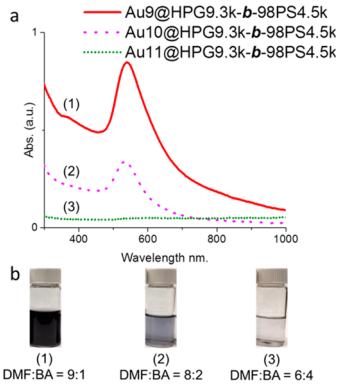

Figure 5. (a) Plasmonic absorption of PS-capped Au nanoparticles templated in the best solvent mixture for PS (i.e., Au9@HPG9.3k-*b*-98PS4.5k in DMF:BA = 9:1) showing a good long-term solution stability, in intermediate solvent mixture for PS (i.e., Au10@HPG9.3k-*b*-98PS4.5k in DMF:BA = 8:2) showing some particle formation and some sedimentation over time, and in the worst solvent mixture for PS (Au11@HPG9.3k-*b*-98PS4.5k in DMF:BA = 6:4) showing no nanoparticle formation and a large-scale aggregation and sedimentation. (b) Digital images of the corresponding PS-capped Au nanoparticles showing their varied solution stability as a function of solvent mixture composition.

reduction in the number of nucleated particles with a noticeable aggregate formation on the bottom of the vial (Figure 5a, middle). Templating in the worst solvent mixture DMF:BA = 6:4 was completely ineffective and TEM was unable to be performed. The immediate large-scale aggregation and sedimentation resulted in a complete loss of nanoscale plasmonic properties as demonstrated by the complete disappearance of the characteristic plasmonic Au peak (Figure 5a, bottom). For comparison, a control experiment was performed in which no template or other surfactant was added (Figure 4c) to emphasize the importance of the HPG-*b*-PS template. Similar to templating in a bad solvent mixture (i.e., DMF:BA = 6:4), the control experiment also showed large-scale agglomeration and sedimentation. Figure 5b shows digital images of the PS-capped Au nanoparticles formed in solvent mixtures of different compositions. Notably, the stability of the PS-capped Au nanoparticles is clearly dependent on the solvent mixture conditions.

Effects of PS Chain Length. It is clear that the solvent composition has a pronounced effect on the success of templating by the HPG-*b*-PS copolymer. This supports the essential role of the PS capping layer during all stages of nanoparticle formation. With this understanding in mind, an initial investigation into the effects of the length and number of the PS chains was undertaken. Four different HPG-*b*-PS templates were studied and used to template Au in DMF. Two templates were derived from HPG10-Br with different lengths of PS chains, and the two other templates were derived from HPG7-Br with different lengths of PS chains (Figure 6). The TEM images demonstrate that the PS chain length does have an effect on the success and quality of templated PS-capped Au nanoparticles. The details of the various PS chain lengths of HPG-*b*-PS templates employed can be found in Table S4 of the Supporting Information. Au12@HPG9.3k-*b*-98PS7k (Figure 6a), Au13@HPG9.3k-*b*-98PS13.4k (Figure 6b), and Au15@HPG12.6k-*b*-117PS5k (Figure 6d) showed aggregate-free templating of Au nanoparticles as demonstrated by the distinct and separate nanoparticles observed. These three samples had

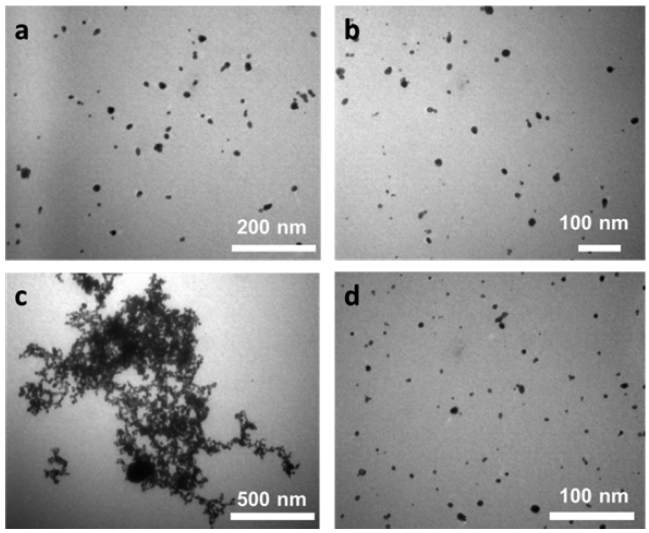

Figure 6. TEM images of Au nanoparticles templated by HPG-*b*-PS of different arm numbers and arm lengths. (a) Au@12HPG9.3k-*b*-98PS7k, HPG9.3k-*b*-98PS7k templated Au nanoparticles (D_{Au} = 12.6 ± 2.0 nm). (b) Au13@HPG9.3k-*b*-98PS13.4k, HPG9.3k-*b*-98PS13.4k templated Au nanoparticles (D_{Au} = 12.9 ± 1.8 nm). (c) Au14@HPG12.6k-*b*-117PS3.6k, HPG12.6k-*b*-117PS3.6k templated Au nanoparticles (aggregated). (d) Au15@HPG12.6k-*b*-117PS5k, HPG12.6k-*b*-117PS5k templated Au nanoparticles (D_{Au} = 6.2 ± 1.3 nm). It is notable that the micrometer-scale aggregation is present in Au14@HPG12.6k-*b*-117PS3.6k. All reactions performed in pure DMF.

PS chain molecular weights ranging from 4500 to 13400 g/mol. Au14@HPG12.6k-*b*-117PS3.6k, which had PS chains with a molecular weight of 3600 g/mol, demonstrated a large-scale aggregation and sedimentation with no solution stability (Figure 6c). This difference between the samples lends support to the importance of the PS capping layer length in minimizing the aggregation and maximizing the separation between the resulting PS-capped Au nanoparticles during both formation and dissolution. This is not surprising as short PS chains (i.e., MW = 3600 g/mol) cannot form a compact layer on the surface of the inner HPG core. As a result, more precursors can diffuse into the space occupied by the inner HPG, resulting in the formation of networklike structures via continuous nucleation and growth of PS-capped colloidal Au nanoparticles.

The effect of arm number on the success of templating appears to be of secondary importance to the lengths of the PS chains. It needs to be emphasized that the initiation efficiency of the PS chains could not be verified due to peak convolution in the ^{1}H NMR. However, it is typical to have high initiation efficiencies in these types of systems based on the reaction conditions. Therefore, nothing definitive can be said about the effect of arm number. The relative importance of arm number will be the subject of future work. The successful nanocomposite formation (defined as well-dispersed aggregate-free templated Au nanoparticles) can also be verified by UV−vis measurement and is consistent with the results observed in TEM (Figure 7a). Specifically, the samples that were well-dispersed showed the expected plasmonic Au peak around 520 nm, whereas the nanoparticles unsuccessfully templated by the short PS chain template produced no such peak and quickly settled out (Figure 7b).

In addition to the spectroscopic and TEM data, it is immediately apparent from examining the solutions which trials were successful and unsuccessful. Since Au is a heavy material,

DOI: 10.1021/acs.langmuir.6b01830
Langmuir 2016, 32, 7180−7188

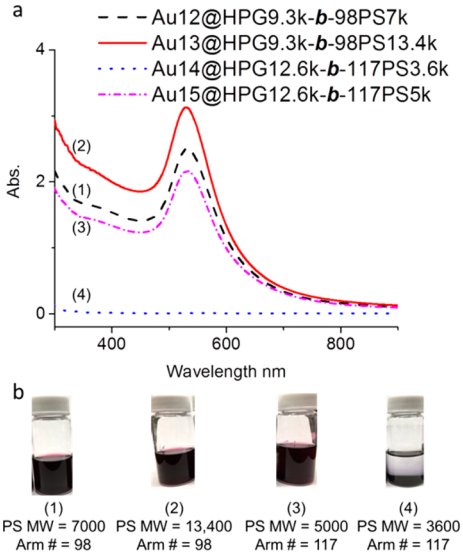

Figure 7. Plasmonic absorption of Au nanoparticles with varied PS arm lengths and arm numbers. Au12@HPG9.3k-*b*-98PS7k, Au13@HPG9.3k-*b*-98PS13.4k, and Au15@HPG12.6k-*b*-117PS5k all showed characteristic plasmonic Au peaks, indicating the successful formation of PS-capped Au nanoparticles with minimal aggregation. Au14@HPG12.6k-*b*-117PS3.6k, which had the shortest PS arm lengths (3600 g/mol), was unable to template Au nanoparticles and thus led to aggregation and absence of plasmonic Au peak.

it settles quickly unless stabilized by a ligand (i.e., CTAB) or long polymer chains. Consequently, particles that are not stabilized quickly aggregate and settle out. In this work, no conventional ligands of any kind were employed and stabilization is only possible when the Au particles are templated using the HPG-*b*-PS template herein devised with relatively long PS chains (MW $\geq$ 4500 g/mol).

CONCLUSIONS

A lower-cost and ligand-free method of templating PS-capped colloidal Au nanoparticles capitalizing on rationally designed unimolecular HPG-*b*-PS copolymers has been devised. The resulting PS-capped Au nanoparticles possessing Au cores below 50 nm in diameter demonstrated excellent solution stability in organic solvents. An investigation of the templating ability of HPG-*b*-PS copolymers was undertaken primarily by tuning the solvent composition and observing the spectroscopic and microscopic data of the resulting PS-capped Au nanoparticles. An initial investigation into the effect of PS arm length was also performed. It was found that the PS arms play the essential role in separating neighboring Au nanoparticles as well as encapsulating the metal ions during nanoparticle formation. When the solvent quality was deliberately worsened, the PS arms were unable to function as intended and the resulting templating ability of the HPG-*b*-PS was reduced and led to the larger aggregates, sedimentation, and ultimately the loss of nanoscale plasmonic properties. The chain length appears to impact the success of Au nanoparticle nucleation and growth. The effect of arm number is likely secondary to the length of the PS chains given that the number of PS arms for all templates investigated is quite large. This simple yet effective strategy for yielding colloidal Au nanoparticles validates the use of polyether coordination as an effective approach in unimolecular polymeric templates.

ASSOCIATED CONTENT

Supporting Information

The Supporting Information is available free of charge on the ACS Publications website at DOI: 10.1021/acs.langmuir.6b01830.

Additional ROMBP reaction details and recipes, sample data and calculation of IG ^{13}C NMR result for HPG2, additional ATRP reaction details as well as recipes and sample labels used in the main text, table summarizing the different sample IDs for different PS-capped Au nanoparticles with different synthesis parameters, digital images showing PS-capped AU nanoparticles successfully templated as well as Au particles not templated and aggregated at the bottom, Raman spectra showing the presence of PS capping layer before and after in situ Au templating, XRD showing characteristic gold peaks present in PS-capped Au nanoparticles (PDF)

AUTHOR INFORMATION

Corresponding Author

*E-mail: zhiqun.lin@mse.gatech.edu.

Notes

The authors declare no competing financial interest.

ACKNOWLEDGMENTS

We would like to thank Professor Holger Frey for his advisement on the HPG synthesis procedure. This work was supported by the Air Force Office of Scientific Research (AFOSR; FA9550-16-1-0187). This work was also supported by the American Society for Engineering Education National Defense Science Engineering Graduate (NDSEG) Fellowship.

REFERENCES

(1) Nam, K. T.; Kim, D.; Yoo, P. J.; Chiang, C.; N, M.; Hammond, P. T.; Chiang, Y.; Belcher, A. M. Virus-enabled Synthesis and Assembly of Nanowires for Lithium Ion Battery Electrodes. *Science* **2006**, *312*, 885−888.

(2) Douglas, T.; Strable, E.; Willits, D.; Aitouchen, A.; Libera, M.; Young, M. Protein Engineering of a Viral Cage for Constrained Nanomaterials Synthesis. *Adv. Mater.* **2002**, *14*, 415−418.

(3) Uchida, M.; Klem, M. T.; Allen, M.; Suci, P.; Flenniken, M.; Gillitzer, E.; Varpness, Z.; Liepold, L. O.; Young, M.; Douglas, T. Biological Containers: Protein Cages as Multifunctional Nanoplatforms. *Adv. Mater.* **2007**, *19*, 1025−1042.

(4) Zhang, M.; Muller, A. H. E. Cylindrical Polymer Brushes. *J. Polym. Sci., Part A: Polym. Chem.* **2005**, *43*, 3461−3481.

(5) Zheng, Z.; Daniel, A.; Yu, W.; Weber, B.; Ling, J.; Muller, A. H. E. Rare-earth Metal Cations Incorporated Silica Hybrid Nanoparticles Templated by Cylindrical Polymer Brushes. *Chem. Mater.* **2013**, *25*, 4585−4594.

(6) Zhang, J.; Coombs, N.; Kumacheva, E.; Lin, Y.; Sargent, E. A New Approach to Hybrid Polymer-Metal and Polymer-Semiconductor Particles. *Adv. Mater.* **2002**, *14*, 1756−1759.

(7) Pang, X.; Zhao, L.; Han, W.; Xin, X.; Lin, Z. A General and Robust Strategy for the Synthesis of Nearly Monodisperse Colloidal Nanocrystals. *Nat. Nanotechnol.* **2013**, *8*, 426−431.

(8) Kramer, R. M.; Li, C.; Carter, D. C.; Stone, M. O.; Naik, R. R. *J. Am. Chem. Soc.* **2004**, *126*, 13282−13286.

(9) Ueno, T.; Suzuki, M.; Goto, T.; Matsumoto, T.; Nagayama, K.; Watanabe, Y. Engineered Protein Cages for Nanomaterial Synthesis. *Angew. Chem., Int. Ed.* **2004**, *43*, 2527−2530.

(10) Jin, Y.; Gao, X. Plasmonic Fluorescent Quantum Dots. *Nat. Nanotechnol.* **2009**, *4*, 571−576.

DOI: 10.1021/acs.langmuir.6b01830
Langmuir 2016, 32, 7180−7188

(11) Suzuki, K.; Sato, S.; Fujita, M. Template Synthesis of Precisely Monodisperse Silica Nanoparticles within Self-Assembled Organometallic Spheres. *Nat. Chem.* **2010**, *2*, 25−29.
(12) Naik, R. R.; Stringer, S. J.; Agarwal, G.; Jones, S. E.; Stone, M. O. Biomimetic Synthesis and Patterning of Silver Nanoparticles. *Nat. Mater.* **2002**, *1*, 169−172.
(13) Braun, E.; Eichen, Y.; Sivan, U.; Ben-Yoseph, G. DNA-Templated Assembly and Electrode Attachment of a Conducting Silver Wire. *Nature* **1998**, *391*, 775−778.
(14) Liu, J.; Geng, Y.; Pound, E.; Gyawali, S.; Ashton, J. R.; Hickey, J.; Woolley, A. T.; Harb, J. N. Metallization of Branched DNA Origami for Nanoelectronic Circuit Fabrication. *ACS Nano* **2011**, *5*, 2240−2247.
(15) Mertig, M.; Colombi Ciacchi, L.; Seidel, R.; Pompe, W.; De Vita, A. DNA as a Selective Metallization Template. *Nano Lett.* **2002**, *2*, 841−844.
(16) Zhao, M.; Sun, L.; Crooks, R. M. Preparation of Cu Nanocluters within Dendrimer Templates. *J. Am. Chem. Soc.* **1998**, *120*, 4877−4878.
(17) Crooks, R. M.; Zhao, M.; Sun, L.; Chechik, V.; Yeung, L. K. Dendrimer-Encapsulated Metal Nanoparticles: Synthesis, Characterization, and Applications to Catalysis. *Acc. Chem. Res.* **2001**, *34*, 181−190.
(18) Mendrek, B.; Trzebicka, B. Synthesis and Characterization of Well-defined Poly(*tert*-butyl acrylate) Star Polymers. *Eur. Polym. J.* **2009**, *45*, 1979−1993.
(19) Jankova, K.; Bednarek, M.; Hvilsted, S. Star polymers by ATRP of Styrene and Acrylates Employing Multifunctional Initiators. *J. Polym. Sci., Part A: Polym. Chem.* **2005**, *43*, 3748−3759.
(20) Doganci, E.; Tasdelen, M. A.; Yilmaz, F. Synthesis of Miktoarm Star-Shaped Polymers with POSS Core via a Combination of CuAAC Click Chemistry, ATRP, and ROP Techniques. *Macromol. Chem. Phys.* **2015**, *216*, 1823−1830.
(21) Matyjaszewski, K. Atom Transfer Radical Polymerization (ATRP): Current Status and Future Perspectives. *Macromolecules* **2012**, *45*, 4015−4039.
(22) Wei, H.; Wang, C. E.; Tan, N.; Boydston, A. J.; Pun, S. H. ATRP Synthesis of Sunflower Polymers using Cyclic Multimacroinitiators. *ACS Macro Lett.* **2015**, *4*, 938−941.
(23) Kautz, H.; Sunder, A.; Frey, H. Control of the Molecular Weight of Hyperbranched Polyglycerols. *Macromol. Symp.* **2001**, *163*, 67−73.
(24) Paulus, F.; Weiss, M. E. R.; Steinhilber, D.; Nikitin, A. N.; Schutte, C.; Haag, R. Anionic Ring-Opening Polymerization Simulations for Hyperbranched Polyglycerols with Defined Molecular Weights. *Macromolecules* **2013**, *46*, 8458−8466.
(25) Sunder, A.; Hanselmann, R.; Frey, H.; Mulhaupt, R. Controlled Synthesis of Hyperbranched Polyglycerols by Ring-Opening Multibranching Polymerization. *Macromolecules* **1999**, *32*, 4240−4246.
(26) Kainthan, R. K.; Muliawan, E. B.; Hatzikiriakos, S. G.; Brooks, D. E. Synthesis, Characterization, and Viscoelastic Properties of High Molecular Weight Hyperbranched Polyglycerols. *Macromolecules* **2006**, *39*, 7708−7717.
(27) Christ, E.; Muller, S.; Berger-Nicoletti, E.; Frey, H. Hydroxyfunctional Oxetane-Inimers with Varied Polarity for the Synthesis of Hyperbranched Polyether Polyols via Cationic ROP. *J. Polym. Sci., Part A: Polym. Chem.* **2014**, *52*, 2850−2859.
(28) Wilms, D.; Wurm, F.; Nieberle, J.; Bohm, P.; Kemmer-Jonas, U.; Frey, H. Hyperbranched Polyglycerols with Elevated Molecular Weights: A Facile Two-step Synthesis Protocol Based on Polyglycerol Macroinitiators. *Macromolecules* **2009**, *42*, 3230−3236.
(29) Sunder, A.; Mulhaupt, R.; Frey, H. Hyperbranched Polyether-Polyols Based on Polyglycerol: Polarity Design by Block Copolymerization with Propylene Oxide. *Macromolecules* **2000**, *33*, 309−314.
(30) Klein, R.; Schull, C.; Berger-Nicoletti, E.; Haubs, M.; Kurz, K.; Frey, H. ABA Triblock Copolymers Based on Linear Poly(oxymethylene) and Hyperbranched Poly(glycerol): Combining Polyacetals and Polyethers. *Macromolecules* **2013**, *46*, 8845−8852.
(31) Sisson, A. L.; Papp, I.; Landfester, K.; Haag, R. Functional Nanoparticles from Dendritic Precursors: Hierarchical Assembly in Miniemulsions. *Macromolecules* **2009**, *42*, 556−559.
(32) Chen, Y.; Shen, Z.; Barriau, E.; Kautz, H.; Frey, H. Synthesis of Multiarm Star Poly(glycerol)-block-poly(2-hydroxyethyl methacrylate). *Biomacromolecules* **2006**, *7*, 919−926.
(33) Sunder, A.; Bauer, T.; Mulhaupt, R.; Frey, H. Synthesis and Thermal Behavior of Esterified Aliphatic Hyperbranched Polyether Polyols. *Macromolecules* **2000**, *33*, 1330−1337.
(34) Wan, D.; Li, Z.; Huang, J. Synthesis of a New Type of Core-Shell Particle from Hyperbranched Polyglycerol. *J. Polym. Sci., Part A: Polym. Chem.* **2005**, *43*, 5458−5464.
(35) Mesias, R.; Murillo, E. Hyperbranched Polyester Polyol Modified with Polylactic Acid. *J. Appl. Polym. Sci.* **2015**, *132*, 41589.
(36) Mecking, S.; Thomann, R.; Frey, H.; Sunder, A. Preparation of Catalytically Active Palladium Nanoclusters in Compartments of Amphophilic Hyperbranched Polyglycerols. *Macromolecules* **2000**, *33*, 3958−3960.
(37) Zhou, L.; Gao, C.; Xu, W. Robust Fe_3O_4/SiO_2-Pt/Au/Pd Magnetic Nanocatalysts with Multifunctional Hyperbranched Polyglycerol Amplifiers. *Langmuir* **2010**, *26*, 11217−11225.
(38) He, M.; Pang, X.; Liu, X.; Jiang, B.; He, Y.; Snaith, H.; Lin, Z. Monodisperse Dual-Functional Upconversion Nanoparticles-Enabled Near-Infrared Organolead Halide Perovskite Solar Cells. *Angew. Chem., Int. Ed.* **2016**, *55*, 4280−4284.
(39) Xu, H.; Xu, Y.; Pang, X.; He, Y.; Jung, Y.; Xia, H.; Lin, Z. A General Route to Nanocrystal Kebabs Periodically Assembled on Stretched Flexible Polymer Shish. *Sci. Adv.* **2015**, *1*, e1500025.
(40) Jiang, B.; Pang, X.; Li, B.; Lin, Z. Organic-Inorganic Nanocomposites via Placing Monodisperse Ferroelectric Nanocrystals in Direct and Permanent Contact with Ferroelectric Polymers. *J. Am. Chem. Soc.* **2015**, *137*, 11760−11767.
(41) Yang, D.; Pang, X.; He, Y.; Wang, Y.; Chen, G.; Wang, W.; Lin, Z. Precisely Size-Tunable Magnetic/Plasmonic Core/Shell Nanoparticles with Controlled Optical Properties. *Angew. Chem., Int. Ed.* **2015**, *54*, 12091−12096.
(42) Xu, H.; Pang, X.; He, Y.; He, M.; Xia, H.; Lin, Z.; Jung, J. An Unconventional Route to Monodisperse and Intimate Semiconducting Organic-Inorganic Nanocomposites. *Angew. Chem., Int. Ed.* **2015**, *54*, 4636−4640.
(43) Zheng, D.; Pang, X.; Wang, M.; He, Y.; Lin, C.; Lin, Z. Unconventional Route to Hairy Plasmonic/Semiconductor Core/Shell Nanoparticles with Precisely Controlled Dimensions and Their Use in Solar Energy Conversion. *Chem. Mater.* **2015**, *27*, 5271−5278.
(44) Lai, C.; Lee, W.; Wu, I.; Kang, C.; Chen, D.; Chen, L.; Chou, P. Highly, Luminescent Homogeneous ZnO Nanoparticles Synthesized *via* Semiconductive Polyalkylthiophene Template. *J. Mater. Chem.* **2009**, *19*, 7284−7289.
(45) Lai, C.; Wu, I.; Kang, C.; Lee, J.; Ho, M.; Chou, P. Homogeneous, Surfactant-free Gold Nanoparticles Encapsulated by Polythiophene Analogues. *Chem. Commun.* **2009**, 1996−1998.
(46) Zhou, L.; Gao, C.; Hu, X.; Xu, W. General Avenue to Multifunctional Aqueous Nanocrystals Stabilized by Hyperbranched Polyglycerol. *Chem. Mater.* **2011**, *23*, 1461−1470.
(47) Jiang, G.; Wang, L.; Chen, W. Synthesis of Multi-arm Star Polystyrene with Hyperbranched Polyether Core. *Eur. Polym. J.* **2006**, *42*, 3333−3340.
(48) Jiang, G.; Wang, L.; Chen, T.; Chen, C.; Yu, H. Synthesis of Multi-arm Star Polystyrene with Hyperbranched Polyester Initiators by Atom Transfer Radical Polymerization. *J. Appl. Polym. Sci.* **2006**, *99*, 728−733.
(49) Liu, C.; Zhang, Y.; Huang, J. Well-defined Star Polymers with Mixed-arms by Sequential Polymerization of Atom Transfer Radical Polymerization and Reverse Addition-Fragmentation Chain Transfer on a Hyperbranched Polyglycerol Core. *Macromolecules* **2008**, *41*, 325−331.

DOI: 10.1021/acs.langmuir.6b01830
Langmuir 2016, 32, 7180−7188